Int. J. Heat Mass Transfer. Vol. 33, No. 6, pp. 1339–1346, 1990
Printed in Great Britain

0017–9310/90 $3.00+0.00

Improving the performance of porous radiant burners through use of sub-micron size fibers

T. W. TONG, S. B. SATHE and R. E. PECK
Department of Mechanical and Aerospace Engineering, Arizona State University, Tempe, AZ 85287, U.S.A.

(*Received* 5 *July* 1989 *and in final form* 6 *October* 1989)

Abstract—An analysis has been carried out to determine the performance of porous radiant burners (PRB) as a function of fiber size. PRB made with silica or alumina fibers are considered. The radiative properties of the fibers are determined using the electromagnetic wave scattering theory for two different characteristic temperatures—1000 and 1500°C. The properties are used in a combined-mode heat transfer model to calculate the amount of energy radiated by the PRB. It is found that fibers smaller than the order of 1 μm in diameter produce significantly higher radiant output. For a characteristic temperature of 1000°C, in some cases, the increase in output is as high as 63 and 109% for silica and alumina fibers, respectively. For a characteristic temperature of 1500°C, the corresponding increases are 72 and 150%, respectively.

1. INTRODUCTION

In a recent study on the heat transfer characteristics of porous radiant burners (PRB), Tong and Sathe [1] found that a smaller single scattering albedo (ω) of the porous matrix would result in higher radiant output. Typically, the porous matrix of PRB is made of cylindrical fibers of several microns in diameter. Since the radiation spectrum involved in the application ranges roughly from 1 to 15 μm in wavelength, the size parameter ($\alpha \equiv \pi D/\lambda$, where D is the fiber diameter and λ is the wavelength of radiation) of the fibers is of the order of one or slightly larger. It has been shown that for a material with a finite but non-zero imaginary part of the complex refractive index, the scattering efficiency (Q_s) is small compared to the absorption efficiency (Q_a) when $\alpha \ll 1$; hence, ω is also small because $\omega = Q_s/(Q_s+Q_a)$ [2]. This suggests that it may be possible to increase the radiant output of PRB by using fibers smaller than those currently used. It is the purpose of this work to establish quantitatively if and by how much the radiant output of PRB can be increased by using smaller fibers.

Before the analysis is presented, a brief description of the operating principle of PRB is in order. A premixed gaseous fuel–air mixture enters a non-combustible porous layer such as that illustrated schematically in Fig. 1. By adjusting the mass flow rate appropriately, combustion can be stabilized inside the porous layer. The burnt gas heats up the porous matrix via convection. The porous matrix in turn radiates the energy away from the porous layer. Heating is provided to a heat load by means of thermal radiation.

2. ANALYSIS

The analysis is based on a heat transfer model that treats combustion as a constant heat source [1]. The theory of electromagnetic wave scattering [2] is used to determine the radiative properties of the fibers. They are then used as input parameters in the heat transfer model to calculate radiant output.

2.1. *Radiative properties of fibers*

This section presents the background on determining the radiative properties of fibers. The fibers are assumed to be circular and infinitely long. For unpolarized incident radiation with wavelength λ, the extinction efficiency Q_e, which is the sum of Q_s and Q_a, and Q_s of a fiber are given by [2]

$$Q_e = \mathrm{Re}\left[b_{01}+2\sum_{n=1}^{\infty} b_{n1}+2\sum_{n=1}^{\infty} a_{n1} +2\sum_{n=1}^{\infty} b_{n2}+a_{02}+2\sum_{n=1}^{\infty} a_{n2}\right]\Big/\alpha \quad (1)$$

$$Q_s = \left[|b_{01}|^2+2\sum_{n=1}^{\infty}|b_{n1}|^2+2\sum_{n=1}^{\infty}|a_{n1}|^2 +2\sum_{n=1}^{\infty}|b_{n2}|^2+|a_{02}|^2+2\sum_{n=1}^{\infty}|a_{n2}|^2\right]\Big/\alpha \quad (2)$$

where a_{n1}, b_{n1}, a_{n2} and b_{n2} are coefficients that depend on the incidence angle Φ, wavelength of radiation λ, fiber diameter D, and the complex refractive index of the fiber. The expressions for a_{n1}, b_{n1}, a_{n2} and b_{n2} can be found in ref. [2]. The efficiencies averaged over all wavelengths and incidence angles are determined according to

$$\bar{z} = \frac{2}{\pi\sigma T_m^4}\int_0^{\pi/2}\int_0^{\infty} z e_b(T_m)\,\mathrm{d}\lambda\,\mathrm{d}\Phi \quad (3)$$

where z represents either Q_e or Q_s, and the overbar indicates averaged values. Note that Planck's function e_b evaluated at some characteristic temperature T_m has

NOMENCLATURE

- a solid surface area per unit volume of solid
- $a_{n,1}$ coefficients (TM mode)
- $a_{n,2}$ coefficients (TE mode)
- $b_{n,1}$ coefficients (TM mode)
- $b_{n,2}$ coefficients (TE mode)
- c specific heat
- D fiber diameter
- D_c critical fiber diameter
- e_b Planck's function
- G non-dimensional emissive power, $\sigma T^4/Qx_3$
- h heat transfer coefficient
- i radiant intensity
- I non-dimensional radiant intensity, i/Qx_3
- k thermal conductivity
- l mean free path
- L_0 average spacing of fibers
- P pressure
- P_1–P_5 non-dimensional parameters as defined in Table 1
- q^r radiative heat flux
- Q heat generation rate per unit volume
- Q^r non-dimensional radiative heat flux, q^r/Qx_3
- Q_o^r non-dimensional radiant output, $Q^r(\xi_3)$
- Q_e extinction efficiency
- Q_s scattering efficiency
- $\bar{Q}_e$ averaged extinction efficiency
- $\bar{Q}_s$ averaged scattering efficiency
- T temperature
- T_m characteristic temperature
- u velocity
- x coordinate
- x_1–x_3 lengths defined in Fig. 1
- z dummy variable in equation (3)
- $\bar{z}$ averaged z.

Greek symbols

- α size parameter
- δ unit step function
- θ non-dimensional temperature, $(T-T_i)/T_i$
- λ wavelength of radiation
- μ, μ' direction cosine
- ξ non-dimensional coordinate, x/x_3
- ρ density
- σ Stefan–Boltzmann constant
- σ_a absorption coefficient
- σ_e extinction coefficient
- $\bar{\sigma}_e$ averaged extinction coefficient
- σ_s scattering coefficient
- τ optical thickness, $(\sigma_a+\sigma_s)x_3$
- ϕ porosity
- Φ incidence angle
- ω single scattering albedo, $\sigma_s/(\sigma_a+\sigma_s)$
- $\bar{\omega}$ averaged single scattering albedo.

Superscripts

- r radiation
- + positive x direction
- − negative x direction.

Subscripts

- b black body or baseline calculation
- e exit
- g gas
- i inlet
- o output
- s solid.

been used as the weighting function in the averaging process. Equations (1)–(3) can be used to compute the averaged efficiencies once D, the complex refractive index of the fiber, and T_m are specified.

The heat transfer model to be employed requires the averaged scattering albedo and the averaged extinction coefficient $\bar{\sigma}_e$ as input properties. The averaged single scattering albedo is

$$\bar{\omega} = \frac{\bar{Q}_s}{\bar{Q}_e} \tag{4}$$

while the averaged extinction coefficient is related to the averaged extinction efficiency by

$$\bar{\sigma}_e = \frac{4\bar{Q}_e(1-\phi)}{\pi D} \tag{5}$$

with ϕ being the porosity.

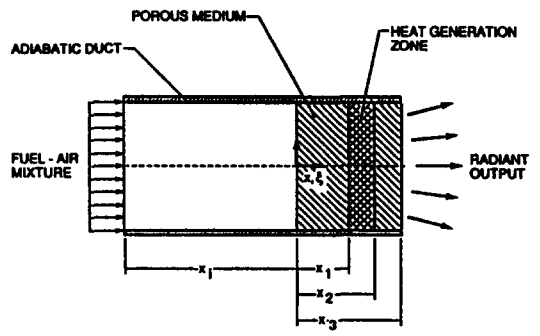

FIG. 1. Schematic diagram of the porous radiant burner.

2.2. *Heat transfer*

The physical situation considered is depicted in Fig. 1. Assuming constant thermophysical properties, steady and laminar slug flow, and one-dimensional radiative heat transfer, one can write the governing equations in dimensionless form as [1]:

energy equation for the gas phase

$$P_1 \frac{d\theta_g}{d\xi} + (1-\phi)P_2(\theta_g - \theta_s) = \phi\delta(\xi) + P_3 \frac{d^2\theta_g}{d\xi^2}; \quad (6)$$

energy equation for the solid phase

$$(1-\phi)P_4 \frac{d^2\theta_s}{d\xi^2} + (1-\phi)P_2(\theta_g - \theta_s) = \frac{dQ^r}{d\xi}; \quad (7)$$

equation of radiative transfer

$$\frac{\mu}{\tau}\frac{\partial I(\xi,\mu)}{\partial \xi} + I(\xi,\mu) = (1-\omega)I_b(\theta_s) + \frac{\omega}{2}\int_{-1}^{1} I(\xi,\mu')\,d\mu'; \quad (8)$$

net radiative heat flux

$$Q^r = 2\pi \int_{-1}^{1} I(\xi,\mu')\mu'\,d\mu'; \quad (9)$$

boundary conditions for the gas phase energy equation

$$\theta_g = 0 \quad \text{at} \quad \xi = -\xi_i \quad (10a)$$

$$\frac{d\theta_g}{d\xi} = 0 \quad \text{at} \quad \xi = \xi_3; \quad (10b)$$

boundary conditions for the solid phase energy equation

$$-\frac{d\theta_s}{d\xi} = P_5(\theta_g - \theta_s) \quad \text{at} \quad \xi = 0 \quad (11a)$$

$$\frac{d\theta_s}{d\xi} = P_5(\theta_g - \theta_s) \quad \text{at} \quad \xi = \xi_3; \quad (11b)$$

boundary conditions for the equation of radiative transfer

$$I^+(0) = 2\int_0^1 I^-(0,-\mu')\mu'\,d\mu' \quad (12a)$$

$$I^-(\xi_3) = \frac{G_e(T_e)}{\pi} \quad (12b)$$

where the dimensionless variables are defined as

$$\xi = x/x_3, \qquad \theta_g = (T_g - T_i)/T_i,$$
$$\theta_s = (T_s - T_i)/T_i, \quad I = i/Qx_3,$$
$$I_b = i_b/Qx_3, \qquad \tau = \sigma_e x_3,$$
$$Q^r = q^r/Qx_3, \qquad G_e = \sigma T_e^4/Qx_3.$$

The definitions of the dimensional variables can be found in the Nomenclature. The physical significance and the definitions of the parameters P_1–P_5 are given in Table 1. Heat generation due to combustion is represented by the term $\phi\delta(\xi)$ in equation (6), where $\delta(\xi)$ is a delta function defined as unity for $\xi_1 \leqslant \xi \leqslant \xi_2$ and zero elsewhere.

Table 1. Significance of P_1–P_5

Parameter	Physical significance
$P_1 = \rho u c_g T_i/Qx_3$	flow enthalpy
$P_2 = haT_i/Q$	convective energy coupling between gas and solid
$P_3 = k_g T_i/Qx_3^2$	gas conduction
$P_4 = k_s T_i/Qx_3^2$	solid conduction
$P_5 = hx_3/k_s$	Biot number

Equation (6) will be applied to the entire domain shown in Fig. 1, that is $-\xi_i \leqslant \xi \leqslant \xi_3$. Accordingly, ϕ is defined such that $\phi = 1$ for $\xi < 0$ and $0 \leqslant \phi \leqslant 1$ for $0 \leqslant \xi \leqslant \xi_3$. Equations (7) and (8) are coupled through equation (9) and they will be used for the porous region. Note that isotropic scattering has been assumed in writing equation (8). This is done because an earlier study [3] demonstrated that anisotropic scattering had less influence on radiant output than other radiation effects, such as a variation in optical thickness and reflection from upstream. As far as the boundary conditions are concerned, equation (10b) specifies that it is adiabatic for the gas at the exit plane. This results from assuming local one way behavior at the outflow position which has been shown by Patankar [4] and Smooke *et al.* [5] to be a reasonable approximation for flow situations such as that being considered. Equations (11a) and (11b) equate the convective heat flux between the gas and solid phases to the conductive heat flux. The upstream radiative boundary condition as indicated by equation (12a) is formulated by characterizing the upstream as a gray and perfectly reflecting surface. Equation (12b) assumes that the burner sees a black environment at T_e.

3. COMPUTATIONS OF THE RADIATIVE PROPERTIES

Both silica and alumina fibers were considered for use as the porous material for the burner. Computations for $\bar{Q}_s$, $\bar{Q}_e$ and $\bar{\omega}_s$ were done by using the trapezoidal rule to approximate the integrals in equation (3). The integrations with respect to Φ were done at 1 degree intervals. The integrations with respect to λ were performed at 0.05 μm intervals with 1 and 16.5 μm chosen as the lower and upper integration limits, respectively. This wavelength range contains 98 and 96% of the black body radiant energy when 1000 and 1500°C, respectively, were employed as T_m. Such a range of characteristic temperatures is representative of the flame temperatures in PRB. For silica fibers the complex refractive index from Malitson [6] for $\lambda < 7$ μm and from Champtier and Friese [7] for $\lambda \geqslant 7$ μm were used. The latter reference also provided the

Table 2. Averaged efficiencies and single scattering albedo of silica fibers, $T_m = 1000°C$

D (μm)	$\bar{Q}_e$	$\bar{Q}_s$	$\bar{\omega}$
5	1.6091	1.5534	0.96540
4	1.6783	1.6261	0.96888
3	1.6990	1.6515	0.97204
2	1.4998	1.4564	0.97107
1	7.5246×10^{-1}	7.2113×10^{-1}	0.95836
0.5	2.3161×10^{-1}	2.1223×10^{-1}	0.91623
0.4	1.3520×10^{-1}	1.1916×10^{-1}	0.88139
0.3	6.0921×10^{-2}	4.8575×10^{-2}	0.79735
0.2	2.1270×10^{-2}	1.2887×10^{-2}	0.60591
0.1	5.6608×10^{-3}	1.4254×10^{-3}	0.25180
0.09	4.8435×10^{-3}	1.0292×10^{-3}	0.21250
0.08	4.1088×10^{-3}	7.1641×10^{-4}	0.17436
0.07	3.4458×10^{-3}	4.7594×10^{-4}	0.13812
0.06	2.8441×10^{-3}	2.9741×10^{-4}	0.10457
0.05	2.2939×10^{-3}	1.7091×10^{-4}	0.07451
0.04	1.7858×10^{-3}	8.6969×10^{-5}	0.04870
0.03	1.3109×10^{-3}	3.6498×10^{-5}	0.02784
0.02	8.6050×10^{-4}	1.0769×10^{-5}	0.01252
0.01	4.2624×10^{-4}	1.3422×10^{-6}	0.00315
0.005	2.1262×10^{-4}	1.6764×10^{-7}	0.00079

Table 3. Averaged efficiencies and single scattering albedo of silica fibers, $T_m = 1500°C$

D (μm)	$\bar{Q}_e$	$\bar{Q}_s$	$\bar{\omega}$
5	1.5715	1.5456	0.98352
4	1.6121	1.5879	0.98499
3	1.7392	1.7173	0.98473
2	1.7445	1.7246	0.98845
1	1.1547	1.1402	0.98750
0.5	4.4964×10^{-1}	4.4073×10^{-1}	0.98017
0.4	2.9451×10^{-1}	2.8713×10^{-1}	0.97495
0.3	1.5339×10^{-1}	1.4771×10^{-1}	0.96297
0.2	4.6254×10^{-2}	4.2397×10^{-2}	0.91663
0.1	6.3525×10^{-3}	4.4038×10^{-3}	0.69324
0.09	4.9123×10^{-3}	3.1573×10^{-3}	0.64274
0.08	3.7440×10^{-3}	2.1832×10^{-3}	0.58311
0.07	2.8079×10^{-3}	1.4414×10^{-3}	0.51336
0.06	2.0673×10^{-3}	8.9560×10^{-4}	0.43322
0.05	1.4888×10^{-3}	5.1198×10^{-4}	0.34389
0.04	1.0409×10^{-3}	2.5929×10^{-4}	0.24909
0.03	6.9473×10^{-4}	1.0837×10^{-4}	0.15598
0.02	4.2284×10^{-4}	3.1867×10^{-5}	0.07536
0.01	1.9946×10^{-4}	3.9622×10^{-6}	0.01986
0.005	9.8248×10^{-5}	4.9449×10^{-7}	0.00503

complex refractive index for alumina for all wavelengths.

4. METHOD OF SOLUTION

Equation (8) was transformed to a set of four first order ordinary differential equations in terms of the moments of the radiant intensity using the P-3 spherical harmonics approximation [3, 8, 9]. Equations (12a) and (12b) were replaced by Marshak's boundary conditions which required the intensity moments to be conserved. The spherical harmonics method and Marshak's boundary conditions for solving the equation of radiative transfer have been well documented elsewhere [3, 8–10]. The readers are referred to these references for the mathematical details. As indicated by equation (9), the first moment of the radiant intensity is the net radiative heat flux.

The four equations governing the moments of the radiant intensity and equations (6) and (7) were solved using an iterative procedure that has been described in detail before [1]. Briefly, it involved guessing $\partial\theta_g/\partial\xi$ at $\xi = 0$, solving the governing equations numerically using DVCPR from the IMSL library, and checking for convergence. Convergence was assumed only when the fractional changes of $\partial\theta_g/\partial\xi$ and θ_g at $\xi = 0$ were both less than 10^{-4}, and an overall energy balance of less than 0.1% was achieved. A relative error tolerance of 10^{-4} was specified for the iterations internal to subroutine DVCPR.

5. RESULTS AND DISCUSSION

The averaged efficiencies and single scattering albedo for silica and alumina fibers can be found in Tables 2–5. The properties were evaluated at characteristic temperatures of 1000°C (Tables 2 and 4) and 1500°C (Tables 3 and 5). The results cover fiber diameters ranging from 0.001 to 5 μm. For both fibers, $\bar{Q}_e$ and $\bar{Q}_s$ may increase and then decrease as the fiber diameter is reduced from 5 μm. This is typical of the oscillatory behavior of the efficiencies when α is of order one or slightly larger [2]. For the approximations used in carrying out the wavelength integral in equation (3) (i.e. 1 and 16.5 μm for the lower and upper limits, respectively), α ranges from 15.71 to 0.95 for a diameter of 5 μm. Even for a smaller diameter such as 1 μm, α is about order one in most of the spectrum since it ranges from 3.14 to 0.19. Therefore, it is clear that for diameters of 1 μm or larger, the efficiencies can be regarded as in the regime where

Table 4. Averaged efficiencies and single scattering albedo of alumina fibers, $T_m = 1000°C$

D (μm)	$\bar{Q}_e$	$\bar{Q}_s$	$\bar{\omega}$
5	1.5204	1.5123	0.99467
4	1.5601	1.5529	0.99537
3	1.6663	1.6598	0.99610
2	1.7765	1.7697	0.99616
1	1.3743	1.3690	0.99615
0.5	5.3004×10^{-1}	5.2050×10^{-1}	0.98191
0.4	3.3431×10^{-1}	3.2511×10^{-1}	0.97247
0.3	1.5532×10^{-1}	1.4909×10^{-1}	0.95987
0.2	4.3107×10^{-2}	3.9940×10^{-2}	0.92654
0.1	5.4371×10^{-3}	4.1072×10^{-3}	0.75539
0.09	4.1262×10^{-3}	2.9429×10^{-3}	0.71321
0.08	3.0743×10^{-3}	2.0333×10^{-3}	0.66139
0.07	2.2438×10^{-3}	1.3414×10^{-3}	0.57983
0.06	1.5999×10^{-3}	8.3281×10^{-4}	0.52054
0.05	1.1104×10^{-3}	4.7597×10^{-4}	0.42848
0.04	7.4545×10^{-4}	2.4085×10^{-4}	0.32309
0.03	4.7720×10^{-4}	1.0063×10^{-4}	0.21088
0.02	2.7969×10^{-4}	2.9589×10^{-5}	0.10579
0.01	1.2842×10^{-4}	3.6790×10^{-6}	0.02865
0.005	6.2786×10^{-5}	4.5914×10^{-7}	0.00731

Table 5. Averaged efficiencies and single scattering albedo of alumina fibers, $T_m = 1500°C$

D (μm)	$\bar{Q}_e$	$\bar{Q}_s$	$\bar{\omega}$
5	1.4586	1.4549	0.99747
4	1.4398	1.4365	0.99772
3	1.5675	1.5646	0.99814
2	1.6946	1.6916	0.99821
1	1.7029	1.7006	0.99864
0.5	8.2748×10^{-1}	8.2334×10^{-1}	0.99499
0.4	5.7336×10^{-1}	5.6939×10^{-1}	0.99307
0.3	3.0259×10^{-1}	2.9990×10^{-1}	0.99111
0.2	9.4844×10^{-2}	9.3476×10^{-2}	0.98557
0.1	9.7215×10^{-3}	9.1463×10^{-3}	0.94084
0.09	7.0249×10^{-3}	6.5131×10^{-3}	0.92715
0.08	4.9227×10^{-3}	4.4725×10^{-3}	0.90854
0.07	3.3233×10^{-3}	2.9330×10^{-3}	0.88256
0.06	2.1424×10^{-3}	1.8107×10^{-3}	0.84514
0.05	1.3035×10^{-3}	1.0290×10^{-3}	0.78941
0.04	7.3666×10^{-4}	5.1839×10^{-4}	0.70373
0.03	3.7653×10^{-4}	2.1568×10^{-4}	0.57281
0.02	1.6992×10^{-4}	6.3201×10^{-5}	0.37194
0.01	5.9670×10^{-5}	7.8375×10^{-6}	0.13135
0.005	2.7939×10^{-5}	9.7769×10^{-7}	0.03499

there is oscillatory behavior. When the diameter is less than 1 μm, there is clearly a monotonic decreasing trend for the averaged efficiencies as the diameter is reduced. Since $\bar{\omega}$ is just the ratio of $\bar{Q}_s$ to $\bar{Q}_e$, it closely follows the trend displayed by the averaged efficiencies.

To illustrate the effect fiber size has on the radiant output, calculations have been performed for decreasing fiber size for three different cases. Case 1: ϕ is kept constant; Case 2: the surface area available for convective heat transfer between the gas and solid phases, that is $(1-\phi)a$, is kept constant; Case 3: both $(1-\phi)a$ and τ are kept fixed. In real situations, all three cases involved increasing the number density of the fibers appropriately. In addition, Case 3 requires increasing the physical thickness of the porous layer.

The input parameters needed to calculate radiant output are shown in Table 6. The parameters in Table 6(a) are those that are kept constant for all the calculations. Their values are chosen to be representative of PRB and have been used in an earlier study [1]. Notice that the flame is assumed to be 0.1 cm thick and is situated in the middle of the porous layer $[(\xi_1+\xi_2)/2 = 0.5]$. In Table 6(b) the parameters that are varied are shown, and the values indicated are used to establish the baseline results that will serve as the data for comparison with the results for smaller diameters.

When D is changed, the parameters affected are τ, ω, and P_2 for Case 1, ϕ, τ, ω, and P_2 for Case 2, and ϕ, x_3, ω, and P_2 for Case 3. It follows from equation (5) that the relationship among τ, x_3, and D is

$$\tau = \frac{4\bar{Q}_e(1-\phi)x_3}{\pi D}. \tag{13}$$

Thus, when a new D is considered, the corresponding $\bar{Q}_e$ from Table 2, 3, 4 or 5 is used in equation (13) to determine τ. Additionally for Case 3, x_3 is adjusted according to the equation to maintain τ constant. Realizing a is equal to $4/D$ and utilizing the definition of P_2 (see Table 1), one can determine P_2 through

$$P_2 = \frac{P_{2b}D_b}{D} \tag{14}$$

where subscript b signifies values used for the baseline calculation, that is values in Table 6(b). For $(1-\phi)a$ to remain the same as that for the baseline calculation, ϕ must be related to D according to

$$\frac{1-\phi}{1-\phi_b} = \frac{D}{D_b}. \tag{15}$$

Equation (15) provides the relation for calculating ϕ for Cases 2 and 3.

Table 6. Input parameters for heat transfer calculations

(a) Parameters that are held constant

	Values used for the present study
x_1 (m)	1
x_3 (cm)	1
x_2-x_1 (cm)	0.1
$(\xi_1+\xi_2)/2$	0.5
P_1	0.01
P_3	2.5×10^{-4}
P_4	0.02
P_5	5
G_e	2.98×10^{-5}

(b) Parameters that are varied

	Values used for the baseline calculation	
	Silica fibers	Alumina fibers
D (μm)	5	5
ϕ	0.95	0.95
τ	193.6	204.9
ω	0.995	0.965
P_2	795	795

Radiant output for silica fibers with $T_m = 1000$ and 1500°C is depicted in Figs. 2 and 3, respectively, and likewise in Figs. 4 and 5 for alumina fibers. The radiant output is presented in a form that the values in the graphs correspond to the fractions of thermal energy generated by combustion. The results for both types of fibers exhibit similar trends (compare Figs. 2 and 4, and Figs. 3 and 5). This is not surprising since $\bar{Q}_e$ and $\bar{\omega}$ for both the fibers exhibit similar behavior as D is decreased. For all three cases the radiant output initially increases slowly or even decreases slightly as D is reduced. This is a result of the oscillatory nature of the efficiencies as discussed earlier. The output increases substantially as D is reduced further. However, it reaches a plateau for Cases 1 and 3 while that for Case 2 drops after reaching a maximum. The plateau occurs when $\bar{\omega}$ is so small that it is no longer an influencing factor and further reduction in fiber size has no impact on the output. This suggests that

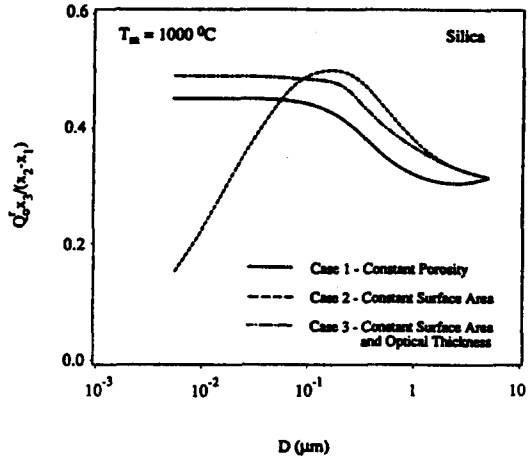

FIG. 2. Radiant output for silica fibers with $T_m = 1000°C$.

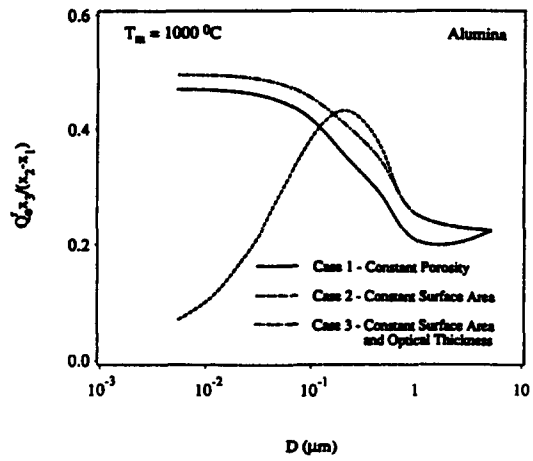

FIG. 4. Radiant output for alumina fibers with $T_m = 1000°C$.

one only needs to reduce the fiber size to the point where the plateau begins to occur. The drop for Case 2 can be explained by the following consideration. Equation (13) indicates that τ is directly proportional to $\bar{Q}_e(1-\phi)$ and inversely proportional to $1/D$. As D is reduced beyond the maximum point, both $\bar{Q}_e$ and $(1-\phi)$ decrease and their product decreases at a faster rate than $1/D$ increases. Hence, one ends up with smaller τ for decreasing D. As demonstrated by Tong and Sathe [1], smaller τ results in lower radiant output.

It is quite apparent that there is a definite advantage in using fibers that are smaller than order of 1 μm in diameter. Based on the plateau values for Cases 1 and 3 and the maximum output for Case 2, the radiant output when compared to the baseline value increases by 42, 54, and 63%, respectively, for silica fibers at $T_m = 1000°C$. The corresponding increases are 61, 72, and 57% for $T_m = 1500°C$. A similar comparison shows 100, 109, and 89% increases, respectively, for alumina fibers at $T_m = 1000°C$, and 140, 150, and 72% increases, respectively, at $T_m = 1500°C$.

Before closing it is worthwhile to note that the results presented were obtained from a continuum model. If the fibers are distributed closer to each other as a result of smaller D, it is possible that the average spacing of the fibers becomes as small as the mean free path of the gas. When this happens the continuum model breaks down and the results presented will no longer be valid. To determine the validity of the results, one needs to compare the average spacing between fibers with the mean free path of the gas. The former depends on how the fibers are distributed. The molecule–fiber collision cross-section is maximized when the fibers are perpendicular to the direction of heat flow. Therefore, as the most stringent condition, the fiber average spacing will be estimated for such a fiber distribution. Assuming the fibers were layered and the axes of the fibers in the same layer were parallel to each other but perpendicular to those in the next layer, Verschoor and Greebler [11] derived the following equation for the fiber average spacing

$$L_0 = \frac{\pi D}{4(1-\phi)}. \tag{16}$$

From kinetic theory the mean free path l of an ideal gas with a molecular diameter of 3.9 Å (diameter of air molecules) is

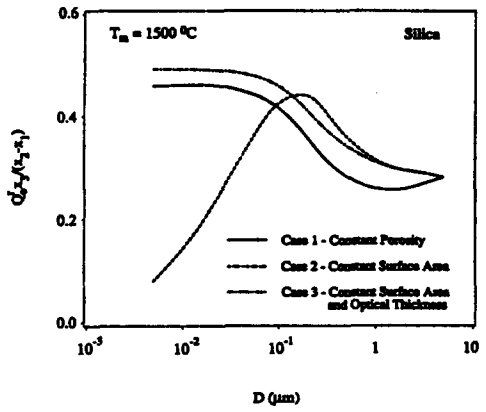

FIG. 3. Radiant output for silica fibers with $T_m = 1500°C$.

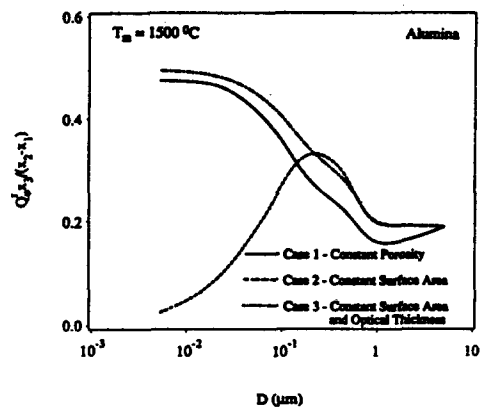

FIG. 5. Radiant output for alumina fibers with $T_m = 1500°C$.

Table 7. D_c for Case 1

T (°C)	P (atm)	D_c (μm)
1000	1	0.0164
	2	0.0082
	3	0.0055
1500	1	0.0229
	2	0.0114
	3	0.0076

$$l = 2.023 \times 10^{-4} \frac{(T+273)}{P} \quad (17)$$

with T in °C and pressure P in atm. Equations (16) and (17) can be used as a guide to estimate the region of validity of the results. First of all, consider Cases 2 and 3. By combining equations (15) and (16), one obtains an equation for L_0 that is in terms of ϕ_b and D_b, but independent of D. Upon substitution of the values in Table 6(b) for ϕ_b and D_b, L_0 turns out to be 78.5 μm. Such a value is much greater than l from equation (17) for $P \geqslant 1$ atm and the two temperatures considered. Hence, the results in Figs. 2–5 for Cases 2 and 3 are always valid. For Case 1, however, L_0 does vary with D according to equation (16). A critical fiber diameter D_c can be defined for $L_0 = l$ and it can be obtained from equations (16) and (17) as

$$D_c = 2.576 \times 10^{-4}(1-\phi)\frac{(T+273)}{P}. \quad (18)$$

Only for $D > D_c$ can results be regarded as meaningful because of the continuum model limitation. Table 7 shows tabulated values of D_c for $\phi = 0.95$, $T = 1000$ and 1500°C, and $P = 1$, 2, and 3 atm. In correlating D_c with the results for Case 1 in Figs. 2–5, it can be seen that D_c for $P = 1$ atm corresponds to a fiber diameter either in the plateau region (Fig. 2) or just when the radiant output is reaching the plateau as D is decreased (Figs. 3–5). For $P = 2$ and 3 atm, D_c lies in the plateau for all of the results in Figs. 2–5. Since $P > 1$ atm for typical PRB operations and one only needs to reduce D to the starting point of the plateau to maximize radiant output, the continuum model limitation can be considered to have no practical impact on the findings for Case 1.

6. CONCLUSIONS

The possibility of using fibers smaller than order of 1 μm in diameter to improve the performance of PRB has been investigated. Based on a one-dimensional conduction, convection, and radiation heat transfer model with spatially dependent heat generation, radiant output for different fiber sizes was computed. The electromagnetic wave scattering theory was used to calculate the radiative properties, which were then used as input parameters in the heat transfer model. The study was carried out for silica and alumina fibers.

It was found that smaller fiber diameters resulted in smaller single scattering albedo and higher radiant output. For both types of fibers, a significant increase in radiant output was found to be possible by reducing the fiber size. For a characteristic temperature of 1000°C increases as large as 63 and 109% were obtained for the silica and alumina fibers, respectively. The corresponding increases at a characteristic temperature of 1500°C were 72 and 150%, respectively.

Acknowledgement—The authors are grateful for the support of this work by the U.S. Department of Energy under contract number DE-FG02-87ER13697.

REFERENCES

1. T. W. Tong and S. B. Sathe, Heat transfer characteristics of porous radiant burners, *ASME HTD* **104**, 147–155 (1988).
2. M. Kerker, *The Scattering of Light*, Chap. 6. Academic Press, New York (1969).
3. T. W. Tong, W. Q. Lin and R. E. Peck, Radiative heat transfer in porous media with spatially dependent heat generation, *Int. Commun. Heat Mass Transfer* **14**, 627–638 (1987).
4. S. V. Patankar, *Numerical Heat Transfer and Fluid Flow*. McGraw-Hill, New York (1980).
5. M. D. Smooke, J. A. Miller and R. J. Kee, Determination of adiabatic flame speeds by boundary value methods, *Combust. Sci. Technol.* **34**, 79–90 (1983).
6. I. H. Malitson, Interspecimen comparison of refractive index of fused silica, *J. Opt. Soc. Am.* **55**, 1205–1209 (1965).
7. R. J. Champtier and G. J. Friese, Use of polished fused silica to standardize directional polarized emittance and reflectance measurements in the infrared, The Aerospace Corporation, Report SAMSO-TR-202 (1974).
8. M. P. Menguc and R. Viskanta, Radiative transfer in three-dimensional rectangular enclosures containing inhomogeneous, anisotropically scattering media, *J. Quant. Spetrosc. Radiat. Transfer* **33**, 533–549 (1985).
9. P. S. Swathi, T. W. Tong and G. R. Cunnington, Jr., Reflectance of two-layer composite porous media with linear-anisotropic scattering, *J. Quant. Spetrosc. Radiat. Transfer* **38**, 273–279 (1987).
10. B. Davidson, *Neutron Transport Theory*. Oxford University Press, Oxford (1957).
11. J. D. Verschoor and P. Greebler, Heat transfer by gas conduction and radiation in fibrous insulations, *Trans. ASME* **74**, 961–968 (1952).

AMELIORATION DES PERFORMANCES DE BRULEURS POREUX RADIANTS PAR UTILISATION DE FIBRES SUBMICRONIQUES

Résumé—On conduit une analyse pour déterminer les performances de brûleurs poreux radiants (PRB) en fonction de la taille des fibres. Les PRB avec des fibres de silice ou d'alumine sont considérés. Les propriétés radiatives des fibres sont déterminées à partir de la théorie de la diffusion des ondes électromagnétiques pour deux températures caractéristiques 1000 et 1500°C. Les propriétés sont utilisées dans un modèle de transferts combinés de chaleur pour calculer la puissance rayonnée par le PRB. On trouve que les fibres plus petites que 1 μm en diamètre donnent des rayonnements sensiblement plus élevés. Pour la température de 100°C, dans certains cas, l'augmentation de puissance est de 63 et 109% respectivement pour des fibres de silice et d'alumine. Pour la température de 1500°C, les accroissements correspondants sont respectivement de 72 et 150%.

LEISTUNGSSTEIGERUNG PORÖSER STRAHLUNGSBRENNER DURCH EINSATZ VON FASERMATERIALIEN IM NANOMETERBEREICH

Zusammenfassung—Die Leistung poröser Strahlungsbrenner wird in Abhängigkeit vom Faserdurchmesser untersucht. Dabei werden Fasern aus Silica und aus Aluminiumoxid verwendet. Die Strahlungseigenschaften der Fasern werden mit Hilfe der Theorie der Streuung elektromagnetischer Wellen bei zwei unterschiedlichen charakteristischen Temperaturen (1000 und 1500°C) untersucht. Diese Eigenschaften werden in einem Modell für kombinierten Wärmetransport verwendet, um den Strahlungsanteil zu berechnen. Es zeigt sich, daß Fasern, deren Durchmesser kleiner als 1 μm ist, signifikant höhere Strahlungsanteile ergeben. Bei der charakteristischen Temperatur 1000°C steigt der Strahlungsanteil in einigen Fällen um 63% (Silicafasern) und 109% (Aluminiumoxidfasern) an. Bei der charakteristischen Temperatur 1500°C ergeben sich Erhöhungen um 72 bzw. 150%.

УЛУЧШЕНИЕ РАБОЧИХ ХАРАКТЕРИСТИК ПОРИСТЫХ РАДИАЦИОННЫХ ГОРЕЛОК С ИСПОЛЬЗОВАНИЕМ ВОЛОКОН СУБМИКРОННОГО РАЗМЕРА

Аннотация—Аналитически определяются рабочие характеристики пористых радиационных горелок (ПРГ) в зависимости от размера волокон пористой вставки. Радиационные свойства волокон устанавливаются с использованием теории рассеяния электромагнитных волн для двух характерных температур—1000 и 1500°C. Эти свойства включены в модель смешанного теплопереноса для расчета излучаемой ПРГ энергии. Найдено, что для волокон с диаметром меньше 1 мкм излучаемая мощность значительно возрастает. В некоторых случаях при характерной температуре 1000°C излучаемая мощность увеличивается на 63 и 109% соответственно для кремнеземных и глиноземных волокон. При характерной температуре 1500°C соответствующие увеличения составляют 72 и 150%.